Supplementary Information

Boosting the capacity of biomass-based supercapacitor using carbon materials of wood derivatives and redox molecules from plants

Tiansheng Wang[a, b, c], Shunyou Hu [b, c], Dong Wu [b, c], Weiwei Zhao[b, c], Wen Yu [b, c], Mi Wang [b, c], Jie Xu[a, c*], Jiaheng Zhang[a, b, c*]

[a]School of Materials Science and Engineering, Harbin Institute of Technology, Harbin 150080, PR China

[b]Sauvage Laboratory for Smart Materials, Harbin Institute of Technology (Shenzhen), Shenzhen 518055, China

[c]School of Materials Science and Engineering, Harbin Institute of Technology (Shenzhen), Shenzhen 518055, China

Corresponding author.

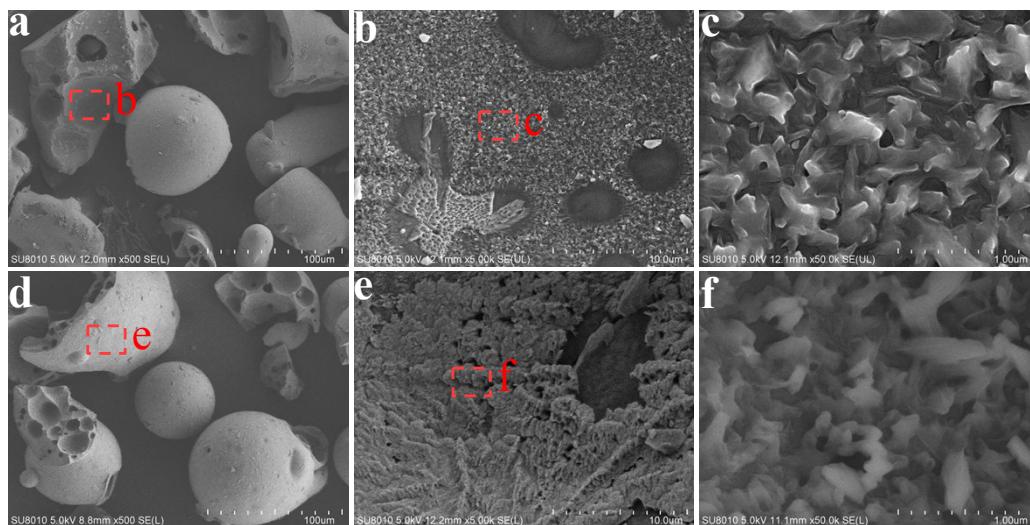***** Email addresses: xjhit@hit.edu.cn; zhangjiaheng@hit.edu.cn

Fig. S1. Typical SEM images of the OLS-1 sample (a–c) and OLS-2 sample (d–f) obtained by LS with molecular weights of 13400 and 4000, respectively: (a, b, d and e) low magnification, (c and f) high magnification.
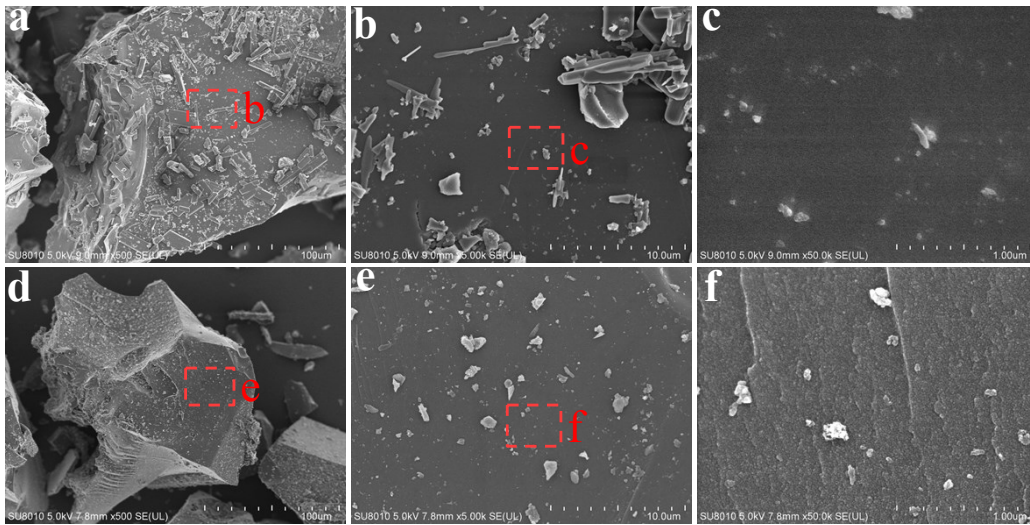
Fig. S2. Typical SEM images of the CLS-1 sample (a–c) and CLS-2 sample (d–f) prepared by OLS-1 and OLS-2, respectively: (a, b, d and e) low magnification, (c and f) high magnification.
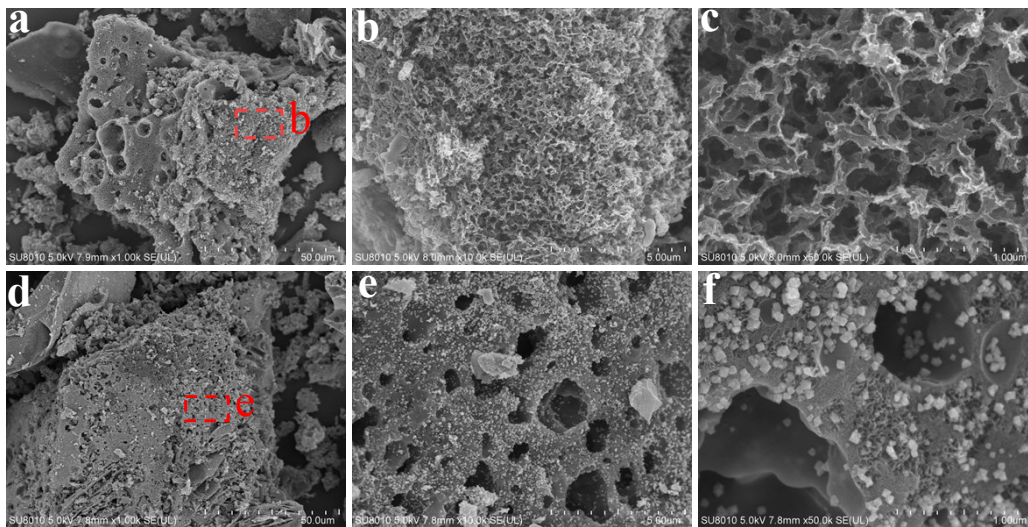
Fig. S3. Typical SEM images of the PGLS-3 sample (a–c) and PGLS-4 sample (d–f) prepared by OLS-1 and OLS-2 through the action of KOH and $FeCl_3$, respectively: (a and d) low magnification, (b, c, e and f) high magnification.
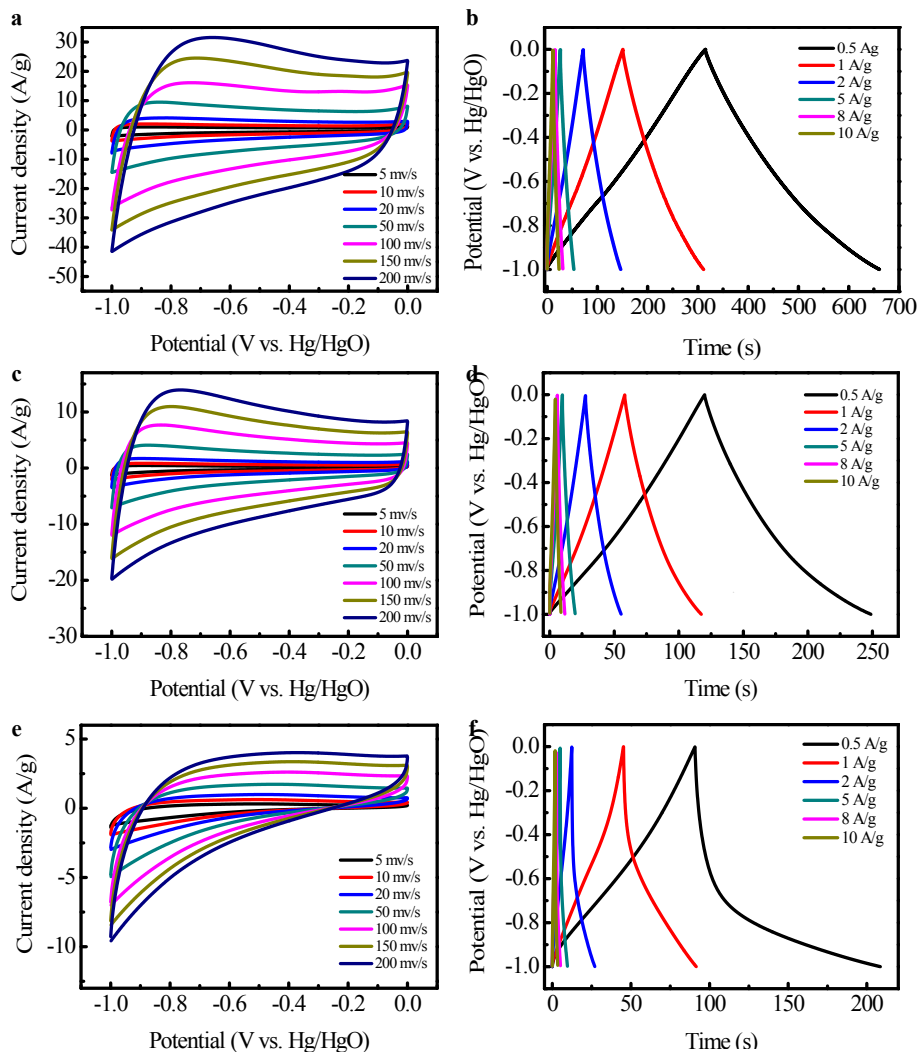
Fig. S4. Electrochemical performance of a single PGLS-1 electrode (a–b), PGLS-3 electrode (c–d) and CLS-1 electrode (e–f) measured in a three-electrode system using 6 M KOH as the electrolyte. (a) The CV profiles of the PGLS-1 electrode collected at different scan rates (from 5 to 200 mV s^{-1}) in the potential range of -1-0 V. (b) The GCD profiles of the PGLS-1 electrode recorded in the potential range of -1-0 V at different current density (from 0.5 to 10 A g^{-1}). (c) The CV profiles of the PGLS-3 electrode collected at different scan rates (from 5 to 200 mV s^{-1}) in the potential range of -1-0 V. (d) The GCD profiles of the PGLS-3 electrode recorded in the potential range of -1-0 V at different current density (from 0.5 to 10 A g^{-1}). (e) The CV profiles of the CLS-1 electrode collected at different scan rates (from 5 to 200 mV s^{-1}) in the potential range of -1-0 V. (f) The GCD profiles of the CLS-1 electrode recorded in the potential range of -1-0 V at different current density (from 0.5 to 10 A g^{-1}).
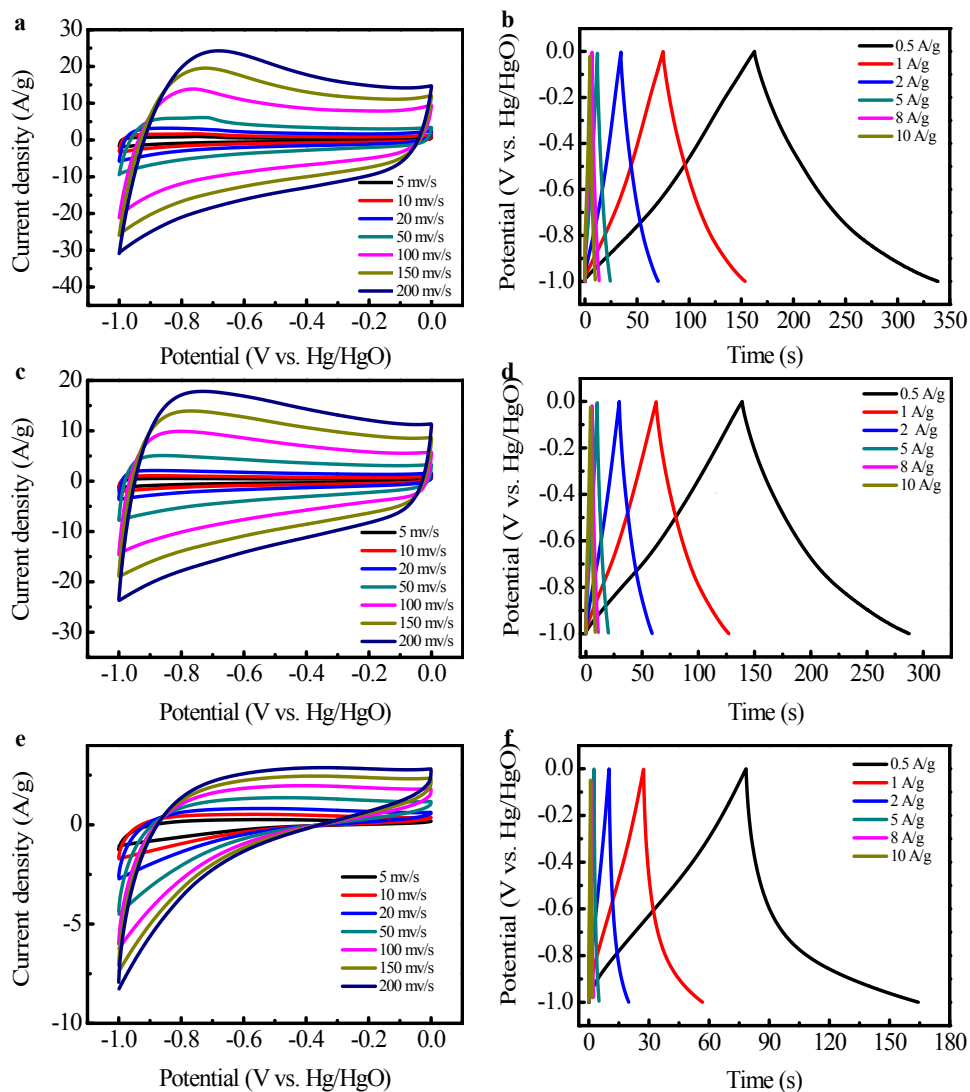
Fig. S5. Electrochemical performance of a single PGLS-2 electrode (a–b), PGLS-4 electrode (c–d) and CLS-2 electrode (e–f) measured in a three-electrode system using 6 M KOH as the electrolyte. (a) The CV profiles of the PGLS-2 electrode collected at different scan rates (from 5 to 200 mV s^{-1}) in the potential range of -1-0 V. (b) The GCD profiles of the PGLS-2 electrode recorded in the potential range of -1-0 V at different current density (from 0.5 to 10 A g^{-1}). (c) The CV profiles of the PGLS-4 electrode collected at different scan rates (from 5 to 200 mV s^{-1}) in the potential range of -1-0 V. (d) The GCD profiles of the PGLS-4 electrode recorded in the potential range of -1-0 V at different current density (from 0.5 to 10 A g^{-1}). (e) The CV profiles of the CLS-2 electrode collected at different scan rates (from 5 to 200 mV s^{-1}) in the potential range of -1-0 V. (f) The GCD profiles of the CLS-2 electrode recorded in the potential range of -1-0 V at different current density (from 0.5 to 10 A g^{-1}).
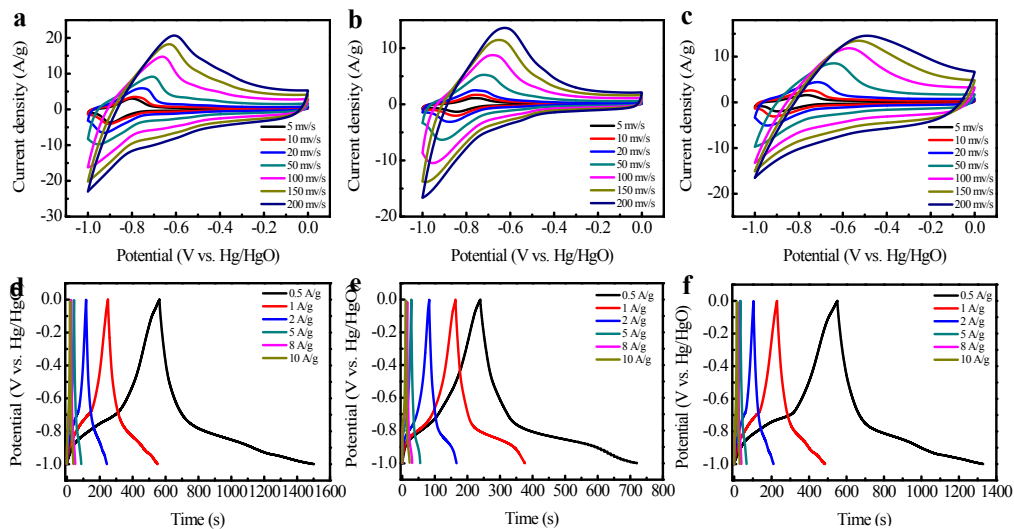
Fig. S6. Electrochemical performance of the composite electrodes with different ARS:PGLS-1 ratios measured in a three-electrode system using 6 M KOH as the electrolyte. The CV profiles of the ARS:PGLS-1=1 (a), ARS:PGLS-1=2 (b) and ARS:PGLS-1=0.5 (c) electrode, respectively, collected at different scan rates (from 5 to 200 mV s^{-1}) in the potential range of -1-0 V. The GCD profiles of the ARS:PGLS-1=1 (d), ARS:PGLS-1=2 (e) and ARS:PGLS-1=0.5 (f) electrode, respectively, recorded in the potential range of -1-0 V at different current density (from 0.5 to 10 A g^{-1}).

Table S1. Pore Structure Parameters of prepared samples calculated from N_2 adsorption isotherms

Samples	[a]S_{BET} (m²/g)	[b]S_{micro} (cm³/g)	[c]S_{ext} (cm³/g)	[d]V_{total} (cm³/g)	[e]V_{micro} (cm³/g)	[f]V_{meso} (cm³/g)	[g]D_{aver} (nm)
CLS-1	55.33	50.69	4.64	0.03	0.01	0.02	2.35
PGLS-3	581.61	459.05	122.56	0.72	0.41	0.31	4.92
PGLS-1	1727.70	1326.32	401.38	1.33	0.73	0.60	3.15
CLS-2	161.69	135.90	25.79	0.09	0.04	0.05	2.30
PGLS-4	596.26	445.74	150.52	0.59	0.30	0.29	3.97
PGLS-2	782.74	633.80	148.94	0.71	0.38	0.33	3.63

[a]Specific surface area (S_{BET}) calculated from the BET method. [b]Micropore specific surface area (S_{micro}) and [c]specific external surface area (S_{ext}) calculated from the N_2 adsorption data. [d]Total pore volume (V_{total}). [e]Micropore volume (V_{micro}) calculated by applying the Dubinin-Radushkevich (D-R) method. [f]Mesopore volume (V_{meso}) calculated by the difference between total pore volume (V_{total}) and micropore volume (V_{micro}). [g]Average pore diameter (D_{aver}).

Electrode Materials	S_{BET} (m^2/g)	Specific capacitance (F/g)	Electrolyte	Cell configuration	Ref.
Porous graphitic bamboo carbon	1732.0	222.0 (0.5 A g^{-1})	6 M KOH	3E	[3]
		48.1 (0.2 A g^{-1})	PVA-KOH	2E	
LS-CNF-PEDOT paper	-	230 (0.5 A g^{-1})	0.1 M HClO$_4$ in	3E	[14]
Lignosulfonate derived hierarchical porous carbons	903.0	247.0 (0.05 A g^{-1})	7 M KOH	2E	[17]
Amorphous microporous carbon	1352.0	61.1 (0.5 A g^{-1})	6 M KOH	2E	[19]
Nitrogen-containing hierarchical porous carbon spheres	1255	276 (0.1A g^{-1})	7 M KOH	3E	[27]
Functional-Group modification of kraft lignin/activated carbon	-	390 (0.5 A g^{-1})	1 M H$_2$SO$_4$	3E	[33]
Cross-linked N-doped carbon nanofiber network	582.0	223.8 (0.5 A g^{-1})	1 M H$_2$SO$_4$	3E	[61]
		53.8 (0.25A g^{-1})	1 M H$_2$SO$_4$	2E	
Biomass based hierarchically porous hollow carbon nanospheres	1984.0	225 (0.2A g^{-1})	6 M KOH	3E	[62]
		40.0 (0.5A g^{-1})	6 M KOH	2E	
3D nanostructure hierarchical porous graphitic carbon from pectin biopolymer	1320.0	274.0 (1A g^{-1})	6 M KOH	3E	[63]
		234.0 (1A g^{-1})	6 M KOH- 1 M Na$_2$SO$_4$	2E	
Nanoporous activated biocarbons	1968.0	223.0 (0.1 A g^{-1})	6 M KOH	2E	[65]
		351.0 (0.1 A g-1)	6 M KOH	3E	
Partially graphitized ginkgo-based activated carbon	1775.0	178.0 (0.4 Ag^{-1})	6 M KOH	3E	[66]
Lignin-derived carbon nanosheets	855.0	281.0 (0.5A g^{-1})	1 M H$_2$SO$_4$	3E	[67]
Graphene hydrogel films	414.0	186.0 (1A g^{-1})	H$_2$SO$_4$-PVA	2E	[68]
ARS/PGLS-1	1727.7	476.5 (0.5A g^{-1})	6 M KOH	3E	This work

Table S2. Specific capacitance of biomass activated carbon reported in the literature

Table S3. Comparison of various carbonaceous electrode based supercapacitors in aqueous electrolyte system

Electrode Materials	Electrolyte	Energy density (Wh/kg)	Power density (W/kg)	Ref.
CNF-PEDOT-ARS	HEC/HClO$_4$/ARS	2.52	1805.0	[2]
Porous graphitic bamboo carbons	PVA/KOH	6.68	100.2	[3]
Lignosulfonate derived porous carbons	KOH	7.02	301.20	[17]
Semi-graphitized microporous carbons	KOH	7.40	151.40	[19]
Nanoporous activated biocarbons	KOH	1.60	10000.00	[60]
Cross-linked N-doped nanofiber network	PVA/H$_3$PO$_4$	5.60	3000.00	[61]
Biomass based hierarchically porous carbon	KOH	5.60	1000.00	[62]
3D nanostructure	KOH	7.90	494.00	[63]
Pyrolyzed activated carbons	Na$_2$SO$_4$	6.50	500.00	[64]
Graphene hydrogel films	PVA/H$_2$SO$_4$	4.50	5000.00	[68]
ARS/PGLS-1	PVA/KOH/ARS	9.45	100.06	This work